Alpha transmitter signal reflection and triggered emissions

Wenyao Gu[1], Lunjin Chen[1], Zhiyang Xia[1], Xin An[2], and Richard B Horne[3]

[1]Physics Department, W. B. Hanson Center for Space Sciences, University of Texas at Dallas, Richardson, Texas, USA
[2]Department of Atmospheric and Oceanic Sciences, UCLA, Los Angeles, CA, USA
[3]British Antarctic Survey, Cambridge, UK

Key Points:

- Both ducted reflected signals and triggered emissions from transmitters are observed in the magnetosphere
- Ducted propagation is suggested using ray tracing model
- Signal time gaps and chirping rate are estimated

Corresponding author: Wenyao Gu, wxg170330@utdallas.edu

Abstract

Russian Alpha radio navigation system (RSDN-20) emits F1=11.9kHz signals into the magnetosphere which propagate as whistler-mode waves. Observed by waveform continuous burst mode from EMFISIS on Van Allen Probes, a case is presented and featured with ducted propagation, multiple reflections and triggered emissions. Both risers and fallers appear in the triggered emissions. We use a ray-tracing method to demonstrate ducted propagation, which has a similar wave normal angle near 150° as the observation. The arrival time of reflected signals is estimated using propagation analysis and compared with the observed signal arrival time. To test the non-linear cyclotron resonance theory, the order of chirping rate in triggered emission is estimated. The estimated order agrees with the observation.

1 Introduction

Signals from VLF transmitters can penetrate the ionosphere inside the transmitter cone and propagate in the magnetosphere in whistler mode, either ducted (Helliwell, 1965) or non-ducted (Cerisier, 1973). In ducted propagation, signals propagate along the field line with nearly parallel wave normal angles. Such propagation requires one-sided or two-sided density structures (Helliwell, 1965) and generally has an upper cut-off frequency of $fce/2$ (half of electron gyrofrequency) (Smith, 1961). In nonducted propagation, wave normal angle can become oblique and even nearly vertical. Reflection happens when wave frequency $f < f_{LHR}$ (lower hybrid resonance frequency) (Kimura, 1966; Edgar, 1972; Kulkarni et al., 2015). Bell et al. (1981) find continuous characteristics of in-situ spatial, amplitude and time delay distributions of signals, and use them as evidences of nonducted waves. Comparing the in-situ observation and the ray tracing group time delays, Rastani et al. (1985) identifies ducted and nonducted transmitter signals. Statistical studies on signal intensities by DEMETER (Clilverd et al., 2008; Z. Zhang et al., 2018) , CREES (Clilverd et al., 2008) and Van Allen Probes (Ma et al., 2017; Z. Zhang et al., 2018) show that nonducted propagation dominates at $L < 1.5$, but there is still controversy on the dominant propagation mode in higher L shells (Agapitov et al., 2014; Ma et al., 2017; Z. Zhang et al., 2018). We need more direct evidences on in-situ wave normal angles to further study ducted and nonducted modes.

Cerisier (1973) indirectly derives in-situ wave normal of transmitter signals using Doppler shift observed by FR-1 on 750km altitude to demonstrate nonducted propagation. For higher altitude observations, Sonwalkar and Inan (1986) use one electric dipole and one magnetic loop antenna to solve the wave normal based on the spinning of DE 1 satellite. With three orthogonal components of magnetic field measurement, Yamamoto et al. (1991) and Kimura et al. (2001) determine the wave normal from Akebono satellite using the technique by Means (1972). In this paper, we use the SVD (singular value decomposition) technique proposed by Santolík et al. (2003) to evaluate the wave normal angle observed by Van Allen Probes.

Triggered emissions of transmitter signals are observed both from ground substantially (Helliwell, 1965; Helliwell & Katsufrakis, 1974; Carpenter & Miller, 1976; Gołkowski et al., 2010; Li et al., 2015) and in space (Bell et al., 1981) with risers, fallers and hooks in the dynamic spectrum. The phenomenon is interpreted by nonlinear cyclotron resonance when electrons are trapped to form an electron hole or hill (clump) in phase space (Omura et al., 1991, 2008). Risers are generated with an electron hole while fallers are generated with an electron hill (Nunn & Omura, 2012; Wang & Berk, 2012).

The observation of ducted propagation accompanied by wave normal characteristics of multiple ducted signals is rarely available in the magnetosphere. In this paper, we present an event of Alpha transmitter signals in the magnetosphere by Van Allen Probes, revealing detailed features associated with ducted propagation. Then a ray tracing model is used to demonstrate the ducted propagation of the transmitter signal. This event, also

accompanied with triggered emissions, provides an unique opportunity to test non-linear cyclotron resonance theory by Omura et al. (2008).

2 Methodology

2.1 Alpha transmitters

Russian Alpha radio navigation system (RSDN-20), which is generally called Alpha transmitters, consists of three stations close to Krasnodar (45°24'N 38°9'E), Novosibirsk (55°45'N 84°27'E) and Khabarovsk (50°4'N 136°36'E) (Jacobsen, 2006). The stations operate at three frequencies: F1=11.90kHz, F2=12.65kHz and F3=14.88kHz. There is a unique pattern for each station at each frequency, with 0.4s signal and 3.6s period. From the statistical observations by DEMETER satellite at an altitude of 660km, the maximum intensities of Alpha signals locate southward of the stations because of field line inclination (X. Zhang et al., 2017). For F1 frequency, the nighttime amplitude near the conjugate points in the southern hemisphere is found to be lower than that above the transmitters (Vavilov et al., 2013). It has been proposed by Vavilov et al. (2013) and X. Zhang et al. (2017) that this phenomenon is due to the magnetospheric reflection above DEMETER orbit (660km) for nonducted waves, where the local LHR frequency is higher than F1 frequency.

2.2 Instrumentation and Data

The Van Allen Probes (formerly Radiation Belt Storm Probes (RBSP)) are two spacecrafts orbiting near the Earth's equatorial plane with 600km perigee, 30,000km apogee and 10° inclination angle. Their waveform continuous burst mode on EMFISIS instrument provides continuous 6s measurement on three orthogonal magnetic and electric field in UVW coordinates with a sampling rate of 35kHz (Kletzing et al., 2013). The UVW coordinate system is defined in Kirby et al. (2014): +W direction is towards the spin axis and +U direction points to the nominal direction of EFW (the Electric Field and Waves Instrument) SPB (spin plane boom) ♯1; +V direction is defined by the right-hand rule. However, a bandpass filter on the instrument completely attenuates F3 frequency signals and partly attenuates F2 frequency pulses (Koronczay et al., 2018). Therefore, we mainly focus on the wave observation at F1 frequency. Figure 1 shows power spectral density of wave electric and magnetic fields captured by the burst mode EMFISIS waveform measurement, illustrating a typical example of Alpha signals in the magnetosphere. The power spectral density is obtained over the 6 seconds through window Fourier transformation with time window of 0.03s and time shift of 0.015s. The signals are from the Novosibirsk station due to the proximity of magnetic longitudes between the satellite location and the transmitter (within 1°). Three components of magnetic field are used in power spectral density calculation, while only EU and EV are used in electric power spectral density calculation due to the large uncertainties in EW component (Wygant et al., 2013). As shown in Figure 1, the 6s waveform is capable of detecting the 2 pulses separated by 3.2s. Therefore, Alpha signals at F1 frequency can be recognized according to the pattern of pulses with 0.4s duration and 3.2s separation. The F2 signals, which are attenuated by the instrument, also follow the same pattern except with a 0.6s lag behind the F1 signals, which is a characteristic of NOV station signals (Jacobsen, 2006). Wave normal angle, ellipticity and planarity are calculated by the singular value decomposition (SVD) method using six components of the electromagnetic field (Santolík et al., 2003). The sign of parallel component of wave vector is decided by the direction of the Poynting vector. We also use Van Allen Probes L4 electron density data, which is inferred from the upper hybrid band (Kurth et al., 2015).

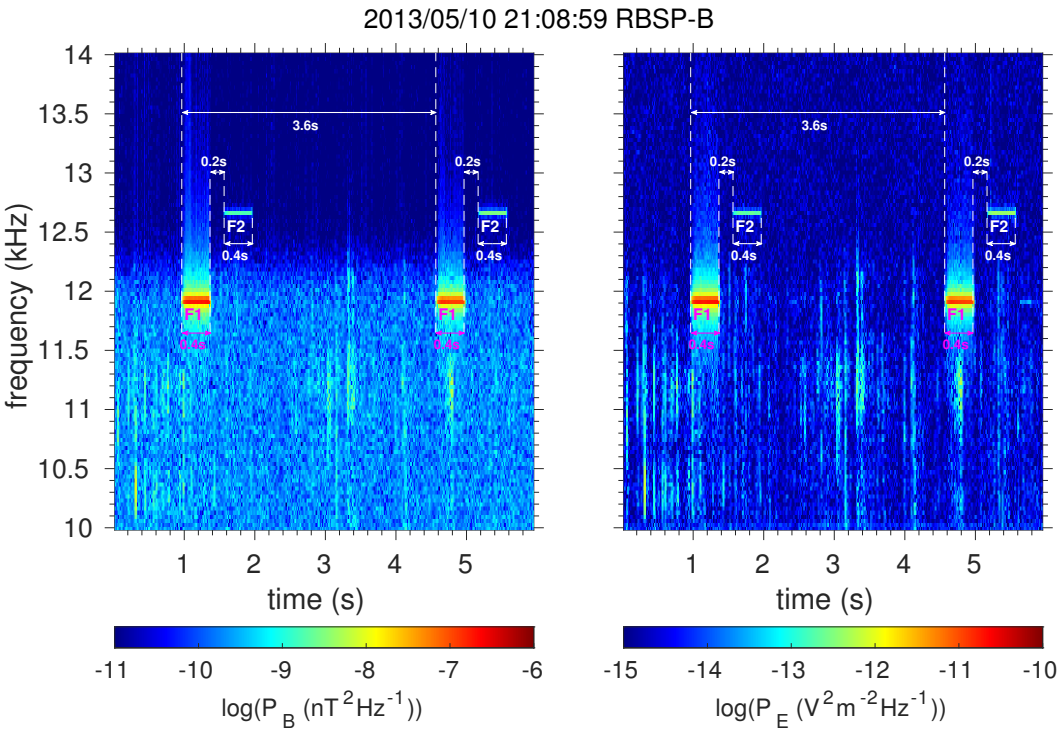

Figure 1. An example of alpha transmitter signals received by RBSPB satellite. The left panel shows the magnetic power spectrum and the right panel shows the electric power spectrum. F1=11.9kHz signals and attenuated F2=12.7kHz signals are shown. White dashed lines show the starting times of the F1 signals. The two F1 signals show the pattern: 0.4s signals with 3.6s period. The F2 signals lag 0.6s behind the F1 signals. The case is observed at MLON=161.9°, close to Novosibirsk (NOV) station at MLON=161.1°.

3 Observation

Figure 2 shows an observation case of Alpha transmitter signals on UT 17:37 2012/11/14 (marked by the vertical red lines), which occurs just after the recovery phase of a geomagnetic disturbance with SYM-H index variation shown in Fig. 2a. The satellite locates inside the plasmasphere of electron density $> 100cm^{-3}$ (Fig. 2b) and of plasmapause location near $L \sim 3$. The electron cyclotron frequency f_{ce} is 140kHz and the lower hybrid frequency $f_{LHR} \approx \sqrt{f_{ce}f_{ci}} = 3.2kHz$, where f_{ci} is the ion cyclotron frequency. The Fourier analysis of the electromagnetic waveform data (Figure 2c-2d) collected at this time (corresponding to magnetic local time ~ 23.7) shows distinct signal pulses occur at F1 and F2 frequencies. Each of them lasts 0.4s, and the separation of the two F2 pulses are about 3.2s, all of which are consistent with the known Alpha transmitter signal pattern. The case locates at magnetic longitude (MLON) $\sim 160.9°$, which is close to the magnetic longitude of NOV station (MLON=161.1°), so the signals are emitted from the NOV transmitter. It is interesting to note that, unlike the usual pattern shown in Figure 1, there are more F1 pulses than F2 pulses (probably because of the instrument attenuation at F2 frequencies) and F1 pulses are separated less than 3.2s. The propagation characteristics are shown in Figure 2e-2j using the SVD method. One can see all the F1 and F2 pulses have positively high ellipticity (Fig. 2e) and high planarity (Fig. 2f), supporting that they are whistler mode waves. The ellipticity and planarity values for all the pulses are shown in Table 1. Wave normal vector direction (Fig. 2g) alternates from antiparallel (or southward direction with $\theta_k = 180°$) and parallel (or northward direction with $\theta_k = 0°$) propagation, where θ_k is polar angle of wave vector with respect to the background magnetic field. The same is true for Poynting vector polar angle θ_p (Fig. 2i). Such alternation of wave normal and Poynting vector directions suggest there exists multiple reflections. Based on the known Alpha transmitter signal pattern and wave normal variation of the pulses, there would be the only interpretation to connecting those pulses below. Therefore, we identify the F1 signal at 37:55.5 (mm:ss) as the original signal from the station that propagates southward, which is labeled by "0" in Fig. 2c. The signals by 1 and 1' have been reflected once from the conjugate point in the southern hemisphere and propagate northward. The signals labeled as 2 and 2' have been reflected for the second time (from the northern hemisphere) and propagate southward. Similarly, the signals labeled 3 and 3' have been reflected for the third time (from the southern hemisphere) and propagate northward. The labels without and with a prime denote two series of original and reflected signals, as the F1 signals are 0.6s ahead of F2 signals in the NOV station (Jacobsen, 2006). Such categorization of the two series is also consistent with observation in Figure 2c-2d that the wave power tends to be weakened in the same series (for example, wave power is the strongest for the signal labeled as 0 while is the weakest for the signal labeled as 3).

We manually acquire the exact starting time of each 0.4s Alpha signal pulse using the magnetic field power spectrum and the polar angle of the Poynting vector. The signal start times are labeled by the black dashed lines in Figure 2. Table 1 summarizes the median values of signal magnetic amplitude, wave normal angle and polar angle of Poynting vector for each identified signal during the 0.4s signal time interval. The magnetic amplitude is calculated from the magnetic power spectrum over a bandwidth of 170Hz. The signals do not strictly follow the guidance along the field line, which would yield 0° and 180° wave normal angles. Instead, the wave normal angles of the southward propagating signals are around 150°, while those of the northward propagating signals are around 20°.

Figure 2c-2d also show the presence of triggered emissions with rising tones in the reflected signals 1', 2', 1, and 2, and falling tones in the reflected signals of the second sequence (1, 2 and 3). There is no triggered emission in the original signal labelled by 0. The triggered emission is generated after the observed original signal "0" but before the observed first reflected signal labelled by "1". So, given the satellite location at MLAT=-

Signal label	Start time (s)	Ellipticity	Planarity	B strength (nT)	Polar k (°)	Polar p (°)
1'	-0.03	0.90	0.85	1.23×10^{-3}	14.1	6.3
2'	0.89	0.81	0.66	9.17×10^{-4}	145.9	152.3
3'	1.59	0.79	0.58	4.11×10^{-4}	21.3	40.3
0	2.78	0.87	0.93	2.39×10^{-3}	150.1	162.8
1	3.54	0.84	0.85	1.29×10^{-3}	17.6	7.4
2	4.45	0.81	0.69	6.70×10^{-4}	145.6	159.0
3	5.24	0.70	0.64	3.44×10^{-4}	26.5	26.3

Table 1. Information in Figure 2. The red color shows the wave normal angles of the southward propagating signals. The blue color shows the wave normal angles of the northward propagating signals.

6°, the interaction region where the triggered emission is formed should be to the south of the satellite position instead of being located exactly at the equator.

4 Estimation

4.1 Propagation time estimate

To account for the gaps between the F1 pulses with alternating propagation directions, we estimate the propagation time delay for reflected signals. Assuming the wave propagation does not deviate much from the field line, the time gaps between the signals in the same time series are estimated using:

$$T = 2 \int_{\lambda_{obs}}^{\lambda_{ref}} \frac{ds}{v_{gz}} \tag{1}$$

, where s is the length of the field line, and $\lambda_{obs} = -6.0°$ is the observation latitude and $\lambda_{ref} = +43.2°$ (for the northward propagation) or $-43.2°$ (for the southward propagation) is the latitude of the ionosphere at an assumed altitude of 100km. The integral is done along the field line of the observation with L=1.91. v_{gz} is the parallel component of the group velocity, which is calculated with the cold plasma dispersion relation. In the calculation, the cold electron density and the wave normal angle are assumed to be the same along the field line (Table 2). The observed time gaps are calculated from start times of the pulses listed in Table 1. Because there is no available density data exactly for the case (Fig. 2b), we use linear interpolation of the logarithmic values of nearby density data within 20 minutes from the case. The interpolation result of $4.3{\times}10^3 cm^{-3}$ gives time gap estimations about half of the observed values (Table 2). Larger value of density is required to obtain a consistent propagation time estimate. The estimated arrival times become close to observations when the density is increased to $1.7{\times}10^4 cm^{-3}$ (Table 2). Such an increase of electron density above the background is also consistent with quasi-ducting of the pulse signals, which forms when there exists a density crest (Smith, 1961).

4.2 Chirping rate of triggered emissions

The chirping rate of triggered emissions is estimated by nonlinear cyclotron resonance theory. The equation of motion for nonlinear cyclotron resonance is (Nunn, 1974; Vomvoridis & Denavit, 1979; Omura et al., 1991):

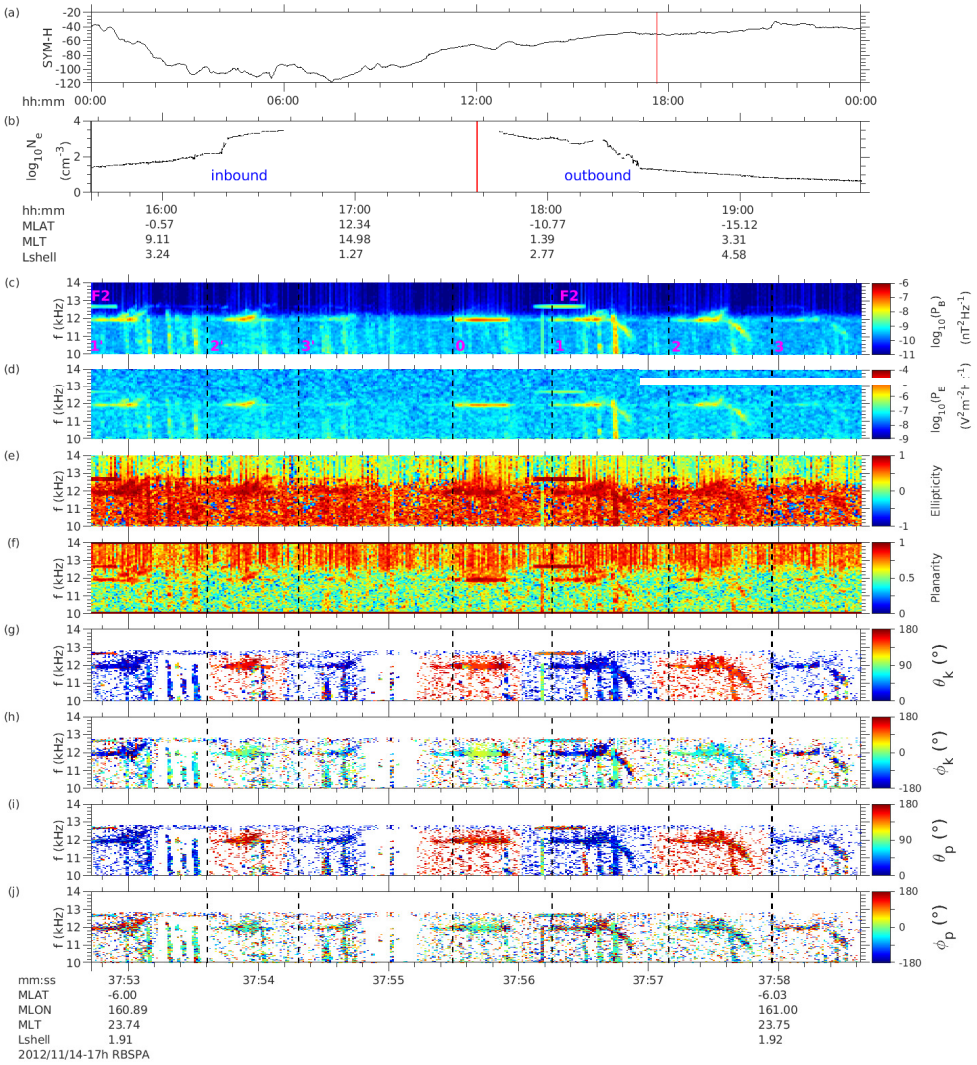

Figure 2. Alpha transmitter signals observed by RBSPA on 2012/11/14. (a) SYM-H of the day. The red line shows the time of the case. (b) Electron density. The red line shows the time of the case. (c) Magnetic field power. (d) Electric field power. (e) Ellipticity. (f) Planarity. (g) Polar angle of k vector. (h) Azimuthal angle of k vector. 0° stands for radially outward. (i) Polar angle of Poynting vector. (j) Azimuthal angle of Poynting vector. 0° stands for radially outward. The signal start times are labeled by black dash lines. F2 signals and the reflection sequences of F1 signals are noted in subplot (c).

Time gap	L shell	Density (cm^{-3})	WNA (°)	Observed time (s)	Estimated time (s)
0∼1	1.9	4.3×10^3	25	0.76	0.34
1∼2	1.9	4.3×10^3	25	0.91	0.50
0∼1	1.9	1.7×10^4	25	0.76	0.67
1∼2	1.9	1.7×10^4	25	0.91	0.99

Table 2. Estimations of the signal time gaps.

$$\frac{du}{dt} = v_\perp \Omega_e \frac{B_\omega}{B} \sin\xi - \frac{v_\perp^2}{2B}\frac{\partial B}{\partial S} - v_\parallel \frac{\partial v_r}{\partial S} - \frac{\dot{\omega}}{k}(1 + \frac{\Omega_e}{2\omega}) \tag{2}$$

, where B_ω is the wave magnetic field strength, B is the background magnetic field. $v_\perp$ and $v_\parallel$ are the perpendicular and the parallel velocities of resonance electrons, respectively. ξ is the phase angle between the wave magnetic field and $v_\perp$. $\Omega_e = \frac{eB}{m_e}$. $u = v_\parallel - v_r$, where the resonance velocity is $v_r = \frac{\omega - \Omega_e}{k}$. On the right-hand side, the first and the second term stand for the wave mirror fore and the dipole mirror force, respectively. The third and the fourth are the non-inertial force terms.

The chirping rate in nonlinear regime is estimated by having the wave mirror term and the non-inertial term with $\dot{\omega}$ being comparable, leading to:

$$\dot{\omega} \sim k v_\perp \Omega_e \frac{B_\omega}{B} \sin\xi \tag{3}$$

, where B_ω is the magnitude of the original signal in Table 1 and B is acquired from the dipole filed at the satellite location. We assume that k is the parallel component of the wave vector and $\sin\xi = 0.4$, which is in the center of the interaction region phase space when nonlinear wave growth reaches maximum (Omura et al., 2008). $v_\parallel = v_\perp = v_r$ is set in resonance condition because the parallel and perpendicular electron velocities generally have the same order. We use a density estimation of $2.0\times10^4 cm^{-3}$ and get the equatorial estimated chirping rate $1\times10^4 Hz/s$. With manually inspections, the observed chirping rate of the falling tones is approximately $4.7\times10^3 Hz/s$, which is at the same order of the estimation. The electron resonance velocity is $v_r = 0.27c$ at the equator. Therefore, the relativistic effect is not necessary to be considered.

5 Discussion

5.1 Ray tracing

We conduct a ray tracing model, using the HOTRAY ray code (Horne, 1989) and a cold plasma density model by Bortnik et al. (2011). The density model consists of a diffusive equilibrium base and adjustable field-aligned structures (Bortnik et al., 2011). Guided by observed density profile (figure 2b), the plasmapause is set at $L_{pp} = (2.7+3.5)/2 = 3.1$ with a width of $0.03R_E$. The plasmapause location is set as the average of the plasmapause locations of the inbound and outbound density profiles (black lines in Figure 3a). A density crest of density $1.7\times10^4 cm^{-3}$, which is suggested by the signal propagation time analysis, is added at the satellite position where $L = 1.9$. The density crest is Gaussian shaped with 400% increase of ambient density and a Gaussian width of $\Delta L = 0.1$. Figure 3a shows the comparison between the model's equatorial cold plasma density profile and two observed profiles (inbound and outbound). Initial locations of rays are set at 700km altitude and at MLAT=41.5° (corresponding to L=1.9), which is within the coverage of F1 frequency observations at NOV station by DEMETER at an altitude of 660km (X. Zhang et al., 2017). Two rays are launched from the two edges of the transmission cone in the meridional plane at F1 frequency respectively. The transmission cone is calculated using a typical nighttime E layer electron number density of $5\times10^4 cm^{-3}$ (Z. Zhang et al., 2018). The simulated ray paths, shown by the blue lines in Figure 3b, are ducted inside the density crest. The wave normal angles of the simulated ducted rays (the blue lines in Figure 3c) oscillate near 180°, and get close to 150° at satellite's latitude (−6°) (Fig. 3c), in accord with the observation. For comparison purpose, two nonducted rays are launched with the initial condition but in the density model with the density crest removed. Unlike ducted rays, the nonducted ray paths (red lines of Figure 3b) deviate significantly from the original field line. The wave normal angles of the nonducted rays are shown by red lines in Figure 3c. At satellite's latitude,

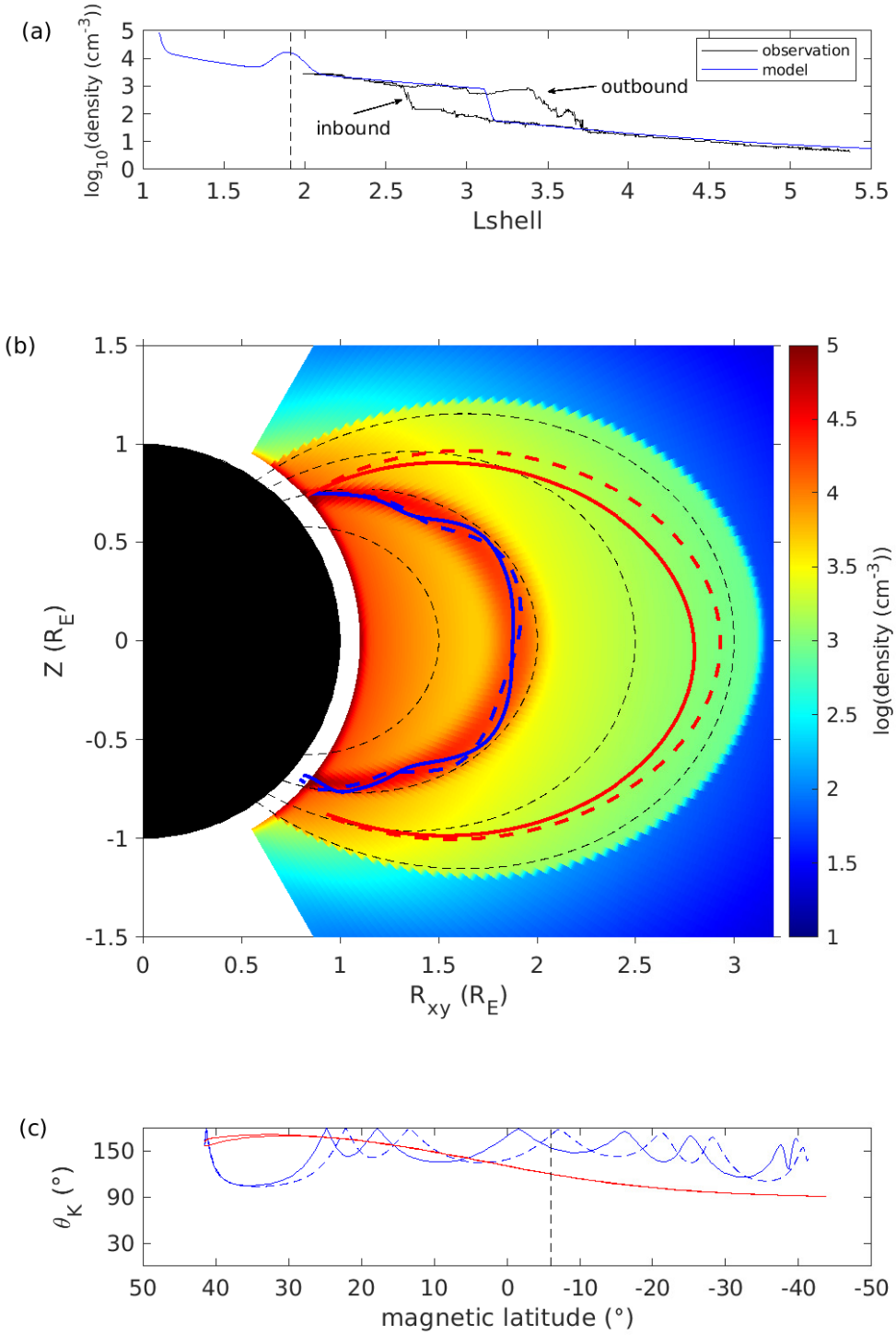

Figure 3. Ray tracing from Novosibirsk station. (a) Observed density profile within 2h from the 2012/11/14 case (black) and equatorial density profile of the ray tracing model (blue). The black dashed line shows the Lshell of the case. (b) Ray tracing of transmitter signals from NOV station. The two blue rays (solid and dashed) are from the edges of the ionospheric transmission cone in the meridional plane. Black dashed lines are the dipole magnetic field lines. Background electron density in the model is shown. The two red rays (sold and dashed) are launched with the same initial condition as the blue rays but in a background electron density model with the duct removed. (c) The two blue line shows the wave normal angles of the two blue rays in subplot (b), while the red line shows the wave normal angles of the two red rays in subplot (b). The solid and dashed lines correspond to the solid and dashed lines in subplot (b) respectively. The two red lines overlap each other. The MLAT of the case is labelled by the black dashed line.

the wave normal angle is near 120°, which is different from the observed values. Such comparison of the wave normal angles and ray paths of ducted and nonducted rays also support the observed case is in a ducted mode.

5.2 Tones of triggered emissions

The inhomogeneity factor S is an important value for nonlinear cyclotron resonance (Omura et al., 1991). The trapping region of the electron in phase space forms where $-1 < S < 1$. At the equatorial upstream, where the signal is propagating from a higher latitude to the equator, the resonant electrons travel in the opposite direction from the equator. S goes from 0 to +1 (Omura et al., 1991) and the phase space trapping region contracts. Therefore, the phase space density increases and an electron hill may form, leading to the generation of falling tones (Nunn & Omura, 2012). Conversely, at the equatorial downstream where the signal is propagating away from the equator, S changes from -1 to 0 and rising tones can be generated by an electron hole (Omura et al., 2008). In the observation, we see rising tones followed by falling tones in the reflected signals at $-6°$ latitude close to the equator. The rising emissions might be triggered with the original reflected signal when they pass through the equatorial region. The falling tone may be triggered at equatorial upstream, when the reflected signal approaches the equator again.

6 Conclusions

1. We perform an observation case of F1 frequency of Alpha transmitters at 11.9kHz by Van Allen Probes. The case shows multiple reflection signals with triggered emissions in the reflected signals.

2. The time gaps of signals are estimated using cold plasma dispersion relations. After adding a density crest, the estimated time gaps agree with the observations.

3. We also do an order estimation of the triggered emission chirping rate to test the nonlinear cyclotron resonance theory. The estimated chirping rate order is in accord with observations.

4. A ray tracing model shows ducted propagation with slightly obique wave normal angle close to 150° at the satellite position, which is similar to the observed values. Therefore, we suggest that the signals propagate in a local density crest.

Acknowledgments
The data of Van Allen Probes used in this paper are provided by Space Physics Data Facility (SPDF) https://spdf.gsfc.nasa.gov/.

References

Agapitov, O. V., Artemyev, A. V., Mourenas, D., Kasahara, Y., & Krasnoselskikh, V. (2014). Inner belt and slot region electron lifetimes and energization rates based on akebono statistics of whistler waves. *Journal of Geophysical Research: Space Physics*, *119*(4), 2876-2893. doi: 10.1002/2014JA019886

Bell, T. F., Inan, U. S., & Helliwell, R. A. (1981). Nonducted coherent vlf waves and associated triggered emissions observed on the isee-1 satellite. *Journal of Geophysical Research: Space Physics*, *86*(A6), 4649-4670. doi: 10.1029/JA086iA06p04649

Bortnik, J., Chen, L., Li, W., Thorne, R. M., & Horne, R. B. (2011). Modeling the evolution of chorus waves into plasmaspheric hiss. *Journal of Geophysical Research: Space Physics*, *116*(A8). doi: 10.1029/2011JA016499

Carpenter, D. L., & Miller, T. R. (1976). Ducted magnetospheric propagation of signals from the siple, antarctica, vlf transmitter. *Journal of Geophysical Research (1896-1977)*, *81*(16), 2692-2700. doi: 10.1029/JA081i016p02692

Cerisier, J. (1973). A theoretical and experimental study of non-ducted vlf waves after propagation through the magnetosphere. *Journal of Atmospheric and Terrestrial Physics*, *35*(1), 77 - 94. doi: https://doi.org/10.1016/0021-9169(73)90217-1

Clilverd, M. A., Rodger, C. J., Gamble, R., Meredith, N. P., Parrot, M., Berthelier, J.-J., & Thomson, N. R. (2008). Ground-based transmitter signals observed from space: Ducted or nonducted? *Journal of Geophysical Research: Space Physics*, *113*(A4). doi: 10.1029/2007JA012602

Edgar, B. (1972, 3). *Structure of the magnetosphere as deduced from magnetospherically reflected whistlers* (Tech. Rep.). Stanford, Calif.: Radiosc. Lab., Stanford Electron. Lab., Stanford Univ.

Gołkowski, M., Inan, U. S., Cohen, M. B., & Gibby, A. R. (2010). Amplitude and phase of nonlinear magnetospheric wave growth excited by the haarp hf heater. *Journal of Geophysical Research: Space Physics*, *115*(A2). doi: 10.1029/2009JA014610

Helliwell, R. A. (1965). *Whistlers and related ionospheric phenomena.* Stanford University Press.

Helliwell, R. A., & Katsufrakis, J. P. (1974). Vlf wave injection into the magnetosphere from siple station, antarctica. *Journal of Geophysical Research (1896-1977)*, *79*(16), 2511-2518. doi: 10.1029/JA079i016p02511

Horne, R. B. (1989). Path-integrated growth of electrostatic waves: The generation of terrestrial myriametric radiation. *Journal of Geophysical Research: Space Physics*, *94*(A7), 8895-8909. doi: 10.1029/JA094iA07p08895

Jacobsen, T. (2006). *The russian vlf navaid system, alpha, rsdn-20.* Retrieved from `http://www.vlf.it/alphatrond/alpha.htm`

Kimura, I. (1966). Effects of ions on whistler-mode ray tracing. *Radio Science*, *1*(3), 269-284. doi: 10.1002/rds196613269

Kimura, I., Kasahara, Y., & Oya, H. (2001). Determination of global plasmaspheric electron density profile by tomographic approach using omega signals and ray tracing. *Journal of Atmospheric and Solar-Terrestrial Physics*, *63*(11), 1157 - 1170. (The Plasmasphere Revisited: A Tribute to Donald Carpenter) doi: https://doi.org/10.1016/S1364-6826(00)00220-0

Kirby, K., Artis, D., Bushman, S., Butler, M., Conde, R., Cooper, S., ... Williams, B. (2014). Radiation belt storm probes—observatory and environments. In N. Fox & J. L. Burch (Eds.), *The van allen probes mission* (pp. 59–125). Boston, MA: Springer US. doi: 10.1007/978-1-4899-7433-4_4

Kletzing, C. A., Kurth, W. S., Acuna, M., MacDowall, R. J., Torbert, R. B., Averkamp, T., ... Tyler, J. (2013, Nov 01). The electric and magnetic field instrument suite and integrated science (emfisis) on rbsp. *Space Science Reviews*, *179*(1), 127–181. doi: 10.1007/s11214-013-9993-6

Koronczay, D., Lichtenberger, J., Juhász, L., Steinbach, P., & Hospodarsky, G. (2018). Vlf transmitters as tools for monitoring the plasmasphere. *Journal of Geophysical Research: Space Physics*, *123*(11), 9312-9324. doi: 10.1029/2018JA025802

Kulkarni, P., Gołkowski, M., Inan, U. S., & Bell, T. F. (2015). The effect of electron and ion temperature on the refractive index surface of 1–10 khz whistler mode waves in the inner magnetosphere. *Journal of Geophysical Research: Space Physics*, *120*(1), 581-591. doi: 10.1002/2014JA020669

Kurth, W. S., De Pascuale, S., Faden, J. B., Kletzing, C. A., Hospodarsky, G. B., Thaller, S., & Wygant, J. R. (2015). Electron densities inferred from plasma wave spectra obtained by the waves instrument on van allen probes. *Journal of Geophysical Research: Space Physics*, *120*(2), 904-914. doi:

10.1002/2014JA020857

Li, J. D., Spasojevic, M., & Inan, U. S. (2015). An empirical profile of vlf triggered emissions. *Journal of Geophysical Research: Space Physics*, *120*(8), 6581-6595. doi: 10.1002/2015JA021444

Ma, Q., Mourenas, D., Li, W., Artemyev, A., & Thorne, R. M. (2017). Vlf waves from ground-based transmitters observed by the van allen probes: Statistical model and effects on plasmaspheric electrons. *Geophysical Research Letters*, *44*(13), 6483-6491. doi: 10.1002/2017GL073885

Means, J. D. (1972). Use of the three-dimensional covariance matrix in analyzing the polarization properties of plane waves. *Journal of Geophysical Research (1896-1977)*, *77*(28), 5551-5559. doi: 10.1029/JA077i028p05551

Nunn, D. (1974). A self-consistent theory of triggered vlf emissions. *Planetary and Space Science*, *22*(3), 349 - 378. doi: https://doi.org/10.1016/0032-0633(74)90070-1

Nunn, D., & Omura, Y. (2012). A computational and theoretical analysis of falling frequency vlf emissions. *Journal of Geophysical Research: Space Physics*, *117*(A8). doi: 10.1029/2012JA017557

Omura, Y., Katoh, Y., & Summers, D. (2008). Theory and simulation of the generation of whistler-mode chorus. *Journal of Geophysical Research: Space Physics*, *113*(A4). doi: 10.1029/2007JA012622

Omura, Y., Nunn, D., Matsumoto, H., & Rycroft, M. (1991). A review of observational, theoretical and numerical studies of vlf triggered emissions. *Journal of Atmospheric and Terrestrial Physics*, *53*(5), 351 - 368. doi: https://doi.org/10.1016/0021-9169(91)90031-2

Rastani, K., Inan, U. S., & Helliwell, R. A. (1985). De 1 observations of siple transmitter signals and associated sidebands. *Journal of Geophysical Research: Space Physics*, *90*(A5), 4128-4140. doi: 10.1029/JA090iA05p04128

Santolík, O., Parrot, M., & Lefeuvre, F. (2003). Singular value decomposition methods for wave propagation analysis. *Radio Science*, *38*(1). doi: 10.1029/2000RS002523

Smith, R. L. (1961). Propagation characteristics of whistlers trapped in field-aligned columns of enhanced ionization. *Journal of Geophysical Research (1896-1977)*, *66*(11), 3699-3707. doi: 10.1029/JZ066i011p03699

Sonwalkar, V. S., & Inan, U. S. (1986). Measurements of siple transmitter signals on the de 1 satellite: Wave normal direction and antenna effective length. *Journal of Geophysical Research: Space Physics*, *91*(A1), 154-164. doi: 10.1029/JA091iA01p00154

Vavilov, D., Shklyar, D., Titova, E., & Parrot, M. (2013). Study of the lower hybrid resonance frequency over the regions of gathering earthquakes using demeter data. *Journal of Atmospheric and Solar-Terrestrial Physics*, *100-101*, 1 - 12. doi: https://doi.org/10.1016/j.jastp.2013.03.019

Vomvoridis, J. L., & Denavit, J. (1979). Test particle correlation by a whistler wave in a nonuniform magnetic field. *The Physics of Fluids*, *22*(2), 367-377. doi: 10.1063/1.862589

Wang, G., & Berk, H. (2012, Sep). Simulation and theory of spontaneous TAE frequency sweeping. *Nuclear Fusion*, *52*(9), 094003. doi: 10.1088/0029-5515/52/9/094003

Wygant, J., Bonnell, J., Goetz, K., Ergun, R., Mozer, F., Bale, S., ... Tao, J. (2013, 12 1). The electric field and waves instruments on the radiation belt storm probes mission. *Space Science Reviews*, *179*(1-4), 183–220. doi: 10.1007/s11214-013-0013-7

Yamamoto, M., Ito, Y., Kishi, Y., Sawada, A., Kimura, I., Nagano, I., ... Hashimoto, K. (1991). k vector measurements of vlf signals by the satellite exos-d. *Geophysical Research Letters*, *18*(2), 325-328. doi: 10.1029/91GL00031

Zhang, X., Zhao, S. F., Ruzhin, Y., Liu, J., & Song, R. (2017). The spatial distribution features of three alpha transmitter signals at the topside ionosphere. *Radio Science*, *52*(5), 653-662. doi: 10.1002/2016RS006219

Zhang, Z., Chen, L., Li, X., Xia, Z., Heelis, R. A., & Horne, R. B. (2018). Observed propagation route of vlf transmitter signals in the magnetosphere. *Journal of Geophysical Research: Space Physics*, *123*(7), 5528-5537. doi: 10.1029/2018JA025637